Combined Quantum Mechanical–Molecular Mechanical Study of Catalysis by the Enzyme Phospholipase A_2: An Investigation of the Potential Energy Surface for Amide Hydrolysis

Bohdan Waszkowycz,†[a] Ian H. Hillier,*[a] Nigel Gensmantel[b] and David W. Payling[b]
[a] *Department of Chemistry, University of Manchester, Manchester M13 9PL, UK*
[b] *Fisons plc, Pharmaceuticals Division, Bakewell Road, Loughborough, Leicestershire LE11 0RH, UK*

A combined *ab initio* molecular orbital–molecular mechanical computational model has been applied to the investigation of the potential energy surface of catalysis by the enzyme phospholipase A_2. By the integration of molecular mechanical and quantum mechanical gradients, the model allows the geometry optimisation of a substrate within the environment of the active site. The method has been applied to a comparison of the mechanisms of ester and amide hydrolysis by phospholipase A_2. An estimation of the transition state for amide hydrolysis is described.

Computational chemistry has contributed significantly to the understanding of many aspects of enzyme catalysis. One of the most successful approaches has been the application of empirical force-field methods (*e.g.* molecular mechanics) together with quantum chemical methods, whether at an *ab initio* or semi-empirical molecular orbital level. Thus molecular mechanics (MM) has been used to model macromolecular structures and energies (*e.g.* to refine the structure of an enzyme–substrate complex), while molecular orbital (MO) methods can be used to evaluate the energies of small fragments of the active site (*e.g.* to estimate the energetics of the processes of bond formation or bond cleavage which characterise the potential energy surface).[1]

The limitations of each method are well known. For example, the MM method cannot be used to investigate the structure and energetics of transition structures along a reaction path, and for many applications is of limited accuracy. On the other hand, a purely MO approach is restricted by computational expense to the evaluation of small supermolecule systems, which, for an enzyme, may represent only a few fragments of the active-site residues.[2] Hence the MO model tends to be a poor approximation of the complex steric and electrostatic environment of the enzyme. These bulk interactions are responsible, for example, for enforcing the structure of catalytic networks within the active site and for the stabilisation of high-energy intermediates. Thus the inclusion of these interactions is of major importance in any description of the catalytic mechanism, as the structure and energy of species which are modelled *in vacuo* may be significantly different from those which arise *in situ* (*i.e.* in the active site).

Here we describe the contribution of bulk steric and electrostatic forces by means of an integrated quantum mechanical–molecular mechanical approach. The important residues of the active site are modelled as a quantum mechanical (QM) supermolecule, which is placed within a large MM system which represents the bulk enzyme. Geometry optimisation of the QM system proceeds by standard analytic gradient methods at an *ab initio* MO level, but is influenced by steric and electrostatic interactions with the MM environment. Thus it is possible to optimise a series of structures upon a potential energy surface, and thereby to model, to a first approximation, the reaction path *in situ*.

A hybrid QM–MM approach has been proposed by other workers, for example in Warshel and Levitt's study of lysozyme.[3] More recently an empirical valence-bond method has been described by Warshel,[4] and also various integrations of MM or molecular dynamics with *ab initio* or semi-empirical MO methods.[5,6] Our work follows the methodology of Singh and Kollman's program QUEST[5] (part of the AMBER[7] suite), with some minor modifications by us.

In the present method, the wavefunction of the QM system is initially calculated either *in vacuo* or within a field of point charges which represent the MM atoms. The incorporation of a field of charges into the QM one-electron Hamiltonian is an efficient method of reproducing the electrostatic interaction of the QM system with the bulk environment, and takes into account the polarisation of the QM system by the active site.[8] The geometry optimisation of the QM atoms is directed by a combination of QM and MM gradients, where the latter are calculated from the standard MM forces which are imposed by the MM environment upon the QM atoms. The QM system is optimised within the field of the stationary MM atoms.

As in our earlier paper,[9] we have applied this QM–MM method to the investigation of the reaction path of substrate hydrolysis within the active site of phospholipase A_2 (PLA2). PLA2 hydrolyses the phospholipids of the cell membrane to release fatty acids (*e.g.* arachidonic acid), and thereby initiates the production of a diverse range of potent cellular mediators such as the prostaglandins.[10] Inhibition of PLA2 is a potentially important route to the treatment of various inflammatory disorders, and therefore an understanding of the mechanism of catalysis may contribute to rational drug design.[11]

Our earlier calculations[9,12] modelled a catalytic mechanism originally proposed by Verheij *et al.*[13] on the basis of the crystal structure of PLA2[14] and on limited experimental evidence, and it was demonstrated that this mechanism was valid on structural and energetic grounds. Since then, the first X-ray structures have become available for enzyme–substrate complexes of a phospholipid inhibitor[15] and a transition state analogue[16] within the active site of PLA2. This has supported the proposed mechanism in terms of the mode of binding of the phospholipid and the nature of the oxyanion intermediate.

PLA2 specifically hydrolyses the 2-acyl ester bond of 1,2-diacyl-*sn*-3-glycerophosphatides (L-α-phospholipids, *e.g.* **1**). The X-ray structures of Thunnissen *et al.*[15] and Scott *et al.*[16] confirmed that the phospholipid binds to the active-site calcium ion *via* the C^2 carbonyl and a phosphoryl oxygen, with a hydrophobic interaction between the C^2 alkyl chain and the wall of the active site. This serves to position the C^2 carbonyl adjacent to a histidine–aspartate couple (His-48 and Asp-99 of bovine pancreatic PLA2), which is proposed to function

† *Present address:* Proteus Molecular Design Ltd, 48 Stockport Road, Marple, Cheshire SK6 6AB, UK.

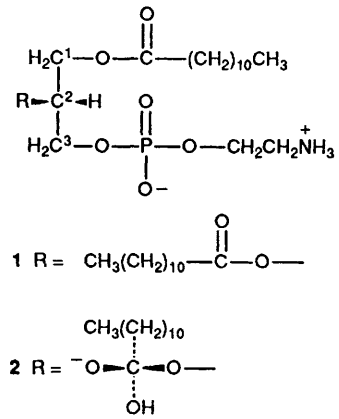

similarly to the Ser–His–Asp triad of the serine proteases. In the case of PLA2, the nucleophile which attacks the C^2 carbonyl is presumed to be a water molecule, which is seen to be hydrogen-bonded to His-48 in the X-ray structure of the uncomplexed enzyme.[14] Attack of this water molecule on the ester carbonyl would be concerted with proton transfer to the imidazole ring of His-48 (Fig. 1). The high-energy oxyanion intermediate which is formed is stabilised by the electrostatic interaction with the calcium ion. Proton transfer from His-48 to the C^2 ether oxygen leads to the breakdown of the oxyanion, and the release of the C^2 fatty acid.

This reaction path was modelled in our previous paper.[9] The QM supermolecule consisted of the imidazole ring of His-48, the nucleophilic water and a small ester substrate (methyl formate). This was geometry-optimised within an MM environ-

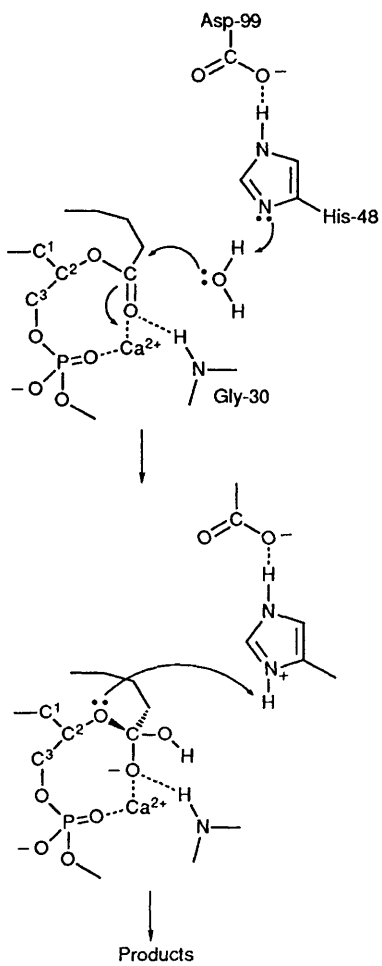

Fig. 1 The proposed mechanism of ester hydrolysis by PLA2

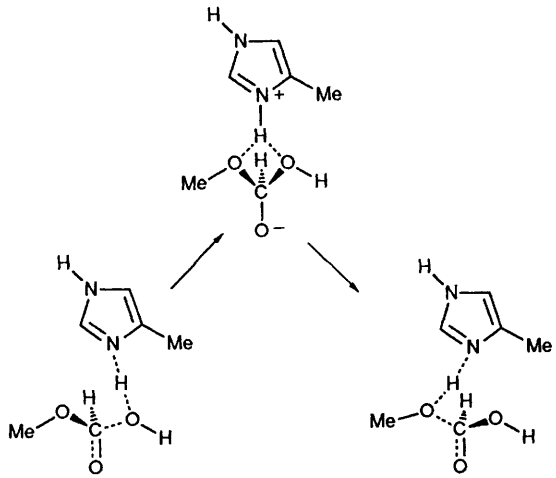

Fig. 2 Schematic representation of the reaction path for proton transfer

ment which represented neighbouring active-site residues. A series of intermediate structures along the reaction path were derived by constraining the distance between the carbonyl carbon and the water oxgen while optimising all other geometric parameters. In this way the reaction path for the attack of water on the ester, leading to the formation of the oxyanion, was modelled. Similarly, the breakdown of the oxyanion into products was modelled by stretching the bond between the carbonyl carbon and the ether oxygen. This is depicted in Fig. 2. Note that it was assumed that the oxyanion intermediate achieves a conformation in which it is doubly hydrogen-bonded to the protonated histidine, *i.e. via* both the water oxygen and the ether oxygen. A doubly hydrogen-bonded oxyanion is generally accepted as the intermediate in ester hydrolysis catalysed by the serine proteases, as it allows a facile proton transfer between the oxygen atoms.[17]

The earlier paper[9] demonstrated that this proton transfer is a valid mechanism, as it occurs across a favourable potential energy surface and requires minimal movement of the substrate or histidine residue. The recent X-ray structure[16] of a phosphonate transition state analogue bound to PLA2 has strongly supported this mechanism by its confirmation that the doubly hydrogen-bonded oxyanion is structurally feasible. Therefore we here employ the same model of the active site in order to compare the earlier results with a further example of substrate hydrolysis. Structural and energetic aspects of amide hydrolysis are considered, as a model of enzyme inhibition. Replacement of the C^2 ester linkage by an amide results in a phospholipid which binds strongly to the active site but is not hydrolysed;[18] we have shown that this may be explained in terms of the resistance to hydrolysis of the amide linkage and the larger binding energy of the amide in comparison with the ester.[12] It has been proposed that amide and ester hydrolysis within the serine proteases proceed by somewhat different mechanisms,[19] and therefore a comparison of the mechanisms of hydrolysis within PLA2 is of interest.

Computational Method.—The modelling of the enzyme–substrate complex and the derivation of the model for the QM–MM optimisations are fully described in our earlier papers.[9,12] In brief, we have used the MM program AMBER to build and minimise structures of phospholipid substrates within the active site of PLA2, which were the basis for MO calculations using the program GAMESS.[20]

An ester phospholipid substrate (1,2-dilauryl-3-*sn*-phosphatidylethanolamine, **1**) was modelled in the extended conformation reported to be present in the lipid membrane,[21] and was

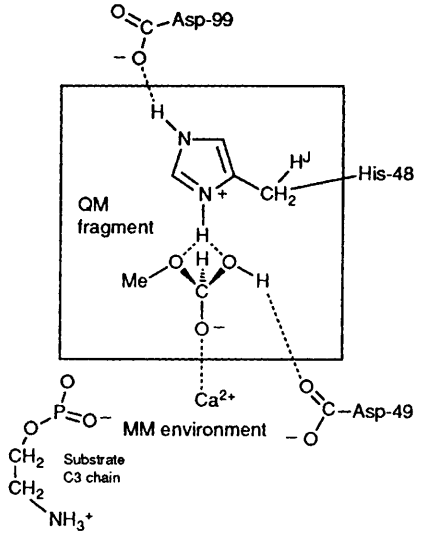

Fig. 3 The partition of the active-site model into QM and MM fragments. Only a few MM residues are depicted. H^J is the (junction) hydrogen which completes the valency of the QM system. The MM substrate fragment omits a phosphoryl oxygen to prevent steric hindrance of the oxyanion.

fitted into the known crystal structure of bovine pancreatic PLA2.[14] This was performed according to the mechanism of Verheij *et al.*,[13] as at the time no X-ray structures of PLA2–substrate complexes were available. For the MM minimisations the entire enzyme was modelled, with an all-atom force-field[22] for the active-site residues (and the substrate), and a united-atom force-field[23] for the bulk of the enzyme. The enzyme was solvated with the 106 water molecules from the original X-ray structure, and a further 640 water molecules added within AMBER to produce a complete solvation shell around the enzyme. Additional MM force-field parameters for the phospholipid were derived from QM optimisations of model structures, and partial charges were determined by the electrostatic potential method of Singh and Kollman[24] with an STO-3G basis set. In a similar way the oxyanion **2**, presumed to be the intermediate which is formed on hydrolysis of the ester **1**, was also modelled.

For the QM–MM optimisations, an active-site model was constructed from the minimised complex of PLA2 and the phospholipid oxyanion. This model comprised 17 active-site amino acids, the calcium ion, four water molecules (which were found to be hydrogen-bonded within the active site) and a small oxyanion, a total of 200 atoms.

A small substrate was used so that the whole of the substrate could be defined as QM atoms, with no junction between the substrate and the MM environment. In this way the freedom of movement of the oxyanion is not restricted by an MM bond to the stationary MM atoms. Therefore the alkyl chains of the full phospholipid were omitted, although the phosphoryl ethylammonium chain was represented by a separate MM fragment (Fig. 3).

The QM atoms of the active-site system were defined as the whole of the oxyanion and the imidazole ring (plus β-methylene group) of His-48; all other atoms were treated as MM. The valency of the β-methylene fragment was filled by the addition of a 'junction' hydrogen atom for the QM calculation. (This hydrogen does not have any bonded or non-bonded MM interactions with the MM atoms. However, unlike the original QUEST program, this hydrogen does interact with the field of MM point charges.)

As before, the hybrid optimisation involved the refinement of the QM atoms in the field of the MM atoms. QM gradients are calculated from the wavefunction of the QM atoms within the field of charges of the MM atoms. To these QM gradients are added the MM gradients imposed by the MM atoms on the QM atoms. The optimisation of the QM atoms proceeds under these combined gradients, while the MM atoms remain stationary.

The MM forces between QM and MM atoms comprise both bonded and non-bonded terms. The movement of the imidazole ring is limited by the MM forces across the QM–MM junction (*i.e.* across the MM bond which connects the His-48 β-carbon and α-carbon), which are the standard MM bond, angle and dihedral forces; the imidazole ring also feels non-bonded interactions with neighbouring residues (van der Waals and hydrogen bond forces). Electrostatic interactions between QM and MM atoms are described only by the incorporation into the one-electron Hamiltonian of the point charges of the MM atoms. The original QUEST program was modified so that all QM atoms intereacted with all MM point charges; the only MM point charge to be omitted was the α-carbon of His-48 (*i.e.* the MM atom which is replaced by the junction hydrogen).

As the oxyanion fragment is not bonded to the MM environment, it is influenced only by non-bonded interactions with the MM atoms. Therefore the oxyanion is allowed considerable freedom of movement within the active site, and its motion is limited only by the balance of its interaction with His-48 and the field of charges (determined by QM) and its interaction with the environment, determined by MM van der Waals and hydrogen bond interactions. The junction hydrogen interacts with the QM atoms and the field of charges but feels no MM forces.

The end result is a first approximation to a QM optimisation *in situ*, rather than *in vacuo*. A benefit of this approach is that no arbitrary constraints need to be imposed to maintain the conformation of the QM system. Attempts were made to optimise the imidazolium–oxyanion couple *in vacuo* using standard QM methods alone, but it was not possible to maintain the intermolecular geometries of the couple without the use of extensive constraints, which necessarily bias any attempt to follow the trajectory of the reaction path towards reactants or products. In the hybrid QM–MM model the dissociation of the dimer is prevented by the MM forces which simulate the interactions with the active site, and thus no arbitrary constraints need be applied to maintain the doubly hydrogen-bonded complex.

In practice, the imidazolium–oxyanion couple was first optimised *in situ* at a 3-21G basis set (123 basis functions). Constraints were used to freeze in space the β-carbon of His-48 and to prevent out-of-plane movement of the imidazolium ring; otherwise all geometric parameters were fully optimised. These constraints are not necessary for the success of the optimisation, since MM forces serve to reproduce the limited movement of the ring within the active site. They were employed here to hasten the convergence of the optimisation, which may otherwise be hampered by small out-of-plane movements of the imidazole ring.

The initial optimisation of the oxyanion–imidazole system in the environment of the active site resulted in a doubly hydrogen-bonded structure described in ref. 9, and labelled as model MIN. This was used to generate a series of intermediate structures along the reaction surface, by means of re-optimisation of the QM system for specific stretches of either the C–OH bond (to model the surface towards the reactants, HCOOMe + HOH) or the C–OMe bond (to model the formation of the products, HCOOH + MeOH) (Fig. 2). With the C–OH and C–OMe bonds being approximately of length 1.45 Å in the fully optimised structure MIN, the intermediate structures were generated for lengths of 1.55, 1.65, 1.75, 1.85 and 2.0 Å. Thus bond stretches of up to approximately 0.5 Å from the optimised geometry were modelled, which enabled the transfer of the

Table 1 Selected geometries for the oxyanion–imidazolium series of structures, for amide hydrolysis within the active site of PLA2. Model MIN is the fully optimised structure, whereas models R1–R5 and P1–P5 represent movement towards reactants or products with the use of constraints on the C–OH or C–N bonds respectively. Model TS is the estimated transition state (see the text). Atom labels are described in Figs. 4 and 7 (Ca is the calcium ion).

	Bond length (Å)					Angle (°)		Dihedral (°)
Model	$C–O^H$	C–N	C–O	Ca–O	$C–N^D$	$O–C–O^H$	O–C–N	$H^N–N–C–O$
R5	2.00	1.343	1.257	2.174	3.77	100.5	121.3	179.1
R4	1.85	1.362	1.269	2.168	3.76	102.7	120.0	−176.7
R3	1.75	1.378	1.280	2.162	3.72	104.2	118.9	−173.9
R2	1.65	1.419	1.301	2.149	3.71	107.9	116.0	−173.1
R1	1.55	1.436	1.315	2.144	3.67	109.0	114.7	−170.9
MIN	1.493	1.485	1.326	2.149	3.45	111.6	116.2	−87.8
P1	1.481	1.55	1.321	2.151	3.45	112.6	115.7	−84.5
P2	1.404	1.65	1.300	2.149	3.67	117.4	110.1	−93.9
P3	1.389	1.75	1.287	2.152	3.71	118.4	109.0	−94.3
P4	1.374	1.85	1.275	2.157	3.74	119.3	107.9	−94.4
P5	1.354	2.00	1.258	2.166	3.78	120.7	105.9	−94.4
TS	1.669	1.402	1.294	2.156	3.67	106.6	117.2	−172.2

Table 2 Selected hydrogen bond geometries for the models of amide hydrolysis

	Bond length (Å)			Angle (°)	Dihedral (°)
Model	$H^T–N^D$	$H^T–O^H$	$H^T–N$	$H^T–N^D–C^G$	$H^T–N^D–C^G–C^D$
R5	1.659	1.001	—	108.3	175.5
R4	1.590	1.020	—	111.6	174.5
R3	1.526	1.042	—	114.3	173.9
R2	1.104	1.411	—	120.2	174.7
R1	1.079	1.463	—	121.2	174.2
MIN	1.046	1.594	2.378	121.9	172.5
P1	1.040	1.627	2.339	122.3	172.3
P2	1.641	—	1.065	138.0	156.5
P3	1.666	—	1.055	139.6	156.6
P4	1.690	—	1.047	141.5	156.9
P5	1.744	—	1.035	144.4	156.8
TS	1.292	1.181	—	118.8	174.4

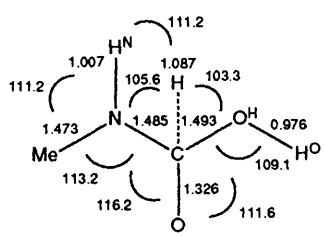

Angles

H–C–O	115.4	N–C–O^H	103.3

Dihedrals

Me–N–C–O^H	−84.3	Me–N–C–O	38.2	H^N–N–C–O	−87.8
Me–N–C–H	167.5	N–C–O^H–H^O	105.5		

Fig. 4 3-21G optimised geometry of the amide oxyanion (model MIN), from the QM–MM optimisation *in situ*. Lengths are quoted in ångströms, angles in degrees.

proton to and from the imidazole ring to be followed. (These structures were labelled R1–R5 for the path towards the reactants, and P1–P5 for the path towards the products; models R5/P5 represented the extreme of reactants/products, with a C–O bond of 2.0 Å.) Thus a set of 10 structures was generated, in which all geometric parameters of the QM system, except for either the C–OH or C–OMe lengths, were fully optimised.

The structure of the MM environment was not altered during the series of optimisations. This is not a significant restriction because no large structural changes occurred to the substrate over the limited reaction path which was considered. Also, the MM parameters of the QM atoms were kept constant for each point: for example, the van der Waals parameters of the carbonyl bond were retained, even though the substrate changed from an ester to an oxyanion and then back to an ester over the reaction path. Modifications to the MM parameters for each structure are valid but would be extremely time-consuming to implement, and may serve to obscure more important features of the calculation.

This procedure was followed for the example described here. The same active-site model was used again, but the ester substrate was replaced by an amide, *N*-methyl formamide. The series of optimisations began with the reactants (point R5), *i.e.* a separation of amide and water of 2.0 Å. (The starting coordinates were derived from the ester system, with the amide assigned a planar structure.) The optimised coordinates of R5 were then used to start point R4, and so on *via* MIN to P5. For each new optimisation, no adjustments were made to the starting conformation which might bias the outcome of the optimisation. Thus there was no re-positioning of the oxyanion or the transferring proton (H^T) in order to achieve proton transfer. However, in some cases it was apparent that there was a small barrier to the transfer of the proton: *i.e.* for a particular $C–O^H$ length, there might be stable minima in which H^T was bonded to O^H or to N^D of His-48 (full atom labels are described in Fig. 7). In these cases, the lower energy structure was chosen.

The calculations were performed on the FPS M64/60 of the Computational Chemistry Group of Manchester University.

Table 3 Energies (kcal mol^{-1}) of models R5–P5 for amide hydrolysis *in situ* (within the active-site model at the 3-21G basis set).[a]

Model	3-21G *in situ* ΔE_{QM}[a]	ΔE_{MM}	ΔE_{TOT}[b]	4-31G *in vacuo*[c] ΔE_{QM}
R5	0.0	0.0	0.0	0.0
R4	+1.50	+0.23	+1.73	+7.77
R3	+2.48	+0.56	+3.04	+14.41
R2	+1.95	+1.43	+3.38	+29.38
R1	+0.35	+1.94	+2.29	+33.05
MIN	−1.31	+1.06	−0.25	+28.45
P1	−0.13	+0.86	+0.73	+29.09
P2	−1.44	+2.11	+0.67	+16.03
P3	+0.41	+1.80	+2.21	+14.21
P4	+3.10	+1.35	+4.45	+12.51
P5	+7.07	+0.57	+7.65	+9.33
TS[d]	+3.43	+0.85	+4.29	+24.44

[a]The energy of the QM supermolecule, E_{QM}, includes the Coulombic interaction of the QM atoms and the MM point charges. [b]E_{TOT} is the sum of E_{QM} and E_{MM}, where E_{MM} is the MM interaction of the QM atoms with the MM atoms (van der Waals, hydrogen bond, and bonded terms). [c]4-31G *in vacuo* energies are for the oxyanion–imidazolium couple with no environment present, and are intended for comparison with the previous model of ester hydrolysis. [d]Model TS is the estimated transition state.

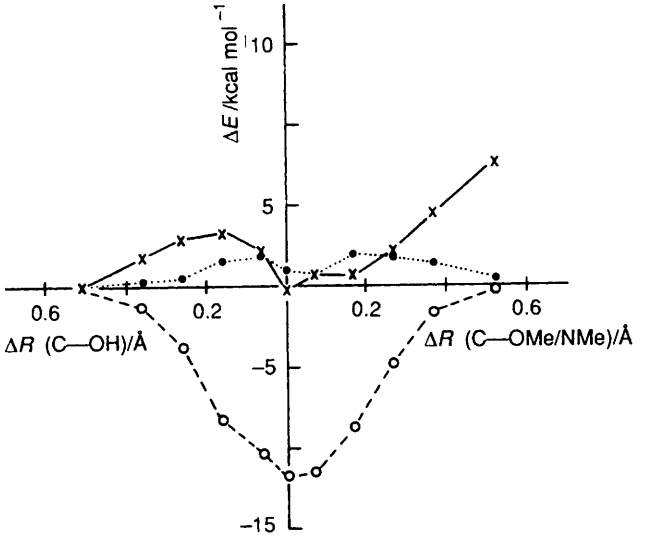

Fig. 5 A plot of the potential energy surface of amide hydrolysis within the active-site model. The curves represent ΔE_{TOT} (solid line) and ΔE_{MM} (dotted line) *in situ*, and for comparison ΔE_{TOT} *in situ* (dashed line) for the ester model (where $\Delta E_{TOT} = \Delta E_{QM} + \Delta E_{MM}$, as in Table 3). ΔR is the stretch of the C–OH or C–N bonds. The origin represents structure MIN, with points to the left representing C–OH stretch, and points to the right C–N stretch. ΔE_{QM} evaluated at 3-21G.

Results and Discussion

Structural Features of Amide Hydrolysis.—The reaction path of amide hydrolysis shows some important differences compared with that obtained for ester hydrolysis. The trajectory of attack of the nucleophilic water molecule (Models R5 to R1) is very similar to the case of ester hydrolysis (Tables 1 and 2, Fig. 4). The nucleophilic water is initially hydrogen-bonded both to His-48 and to a carboxylate oxygen of Asp-49 (one of the metal ligands). The position of O^H changes very little over the sequence of structures, and therefore the reaction path is seen to involve the movement of the substrate towards a stationary nucleophilic water molecule, rather than the attack of the water on the substrate.

For the amide model, proton transfer from water to imidazole

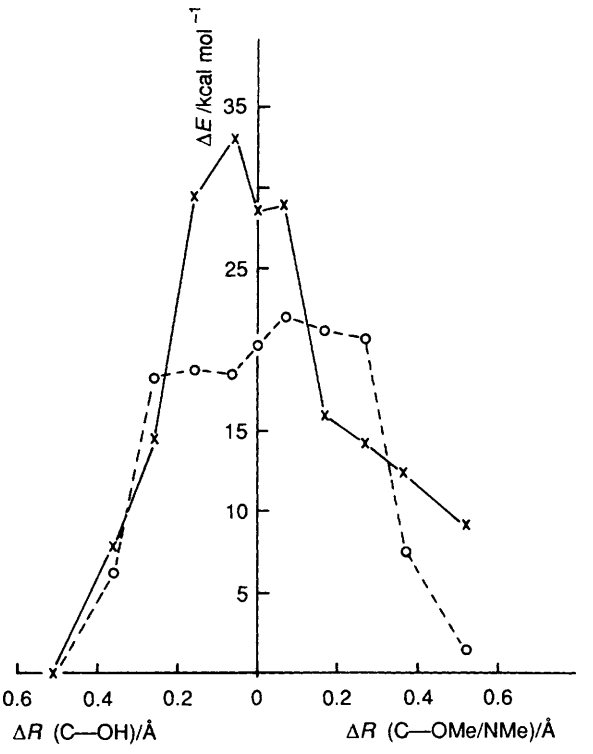

Fig. 6 A plot of the potential surface of amide hydrolysis *in vacuo*, *i.e.* with the structures of the oxyanion–imidazolium couple (generated *in situ*) now evaluated *in vacuo*. The curves compare the energy ΔE_{QM} of the structures obtained for the amide (solid line) with those from the ester model (dashed line).

occurs at a shorter C–O^H distance than for the ester, *i.e.* between 1.65 and 1.75 Å rather than between 1.75 and 1.85 Å as in ester hydrolysis. This is indicative of the relative resistance to nucleophilic attack of the amide (because of the consequent loss of the resonance stability of the amide linkage). As in the case of ester hydrolysis, proton transfer from O^H to N^D is concerted with the formation of the C–O^H bond. It is seen that proton transfer is achieved with no significant movement of the imidazole ring, but relies on the opening-up of the angle H^T–N^D–C^G which the proton makes to the imidazole ring.

Point R1 of the amide model was used as the starting structure for the optimisation of the oxyanion (point MIN), by means of re-optimisation of the structure without the constraint on the C–OH bond. However, point R1 itself proved to be a minimum and no significant change occurred during optimisation. The reason why a structure as distorted as R1 should be a stable minimum is a reflection of the stabilisation of the planar amide linkage. Between point R5 to R1 there is very little distortion of the amide from planarity (the amide dihedral H^N–N–C–O is −171° in R1), even though by point R1 the carbonyl carbon would be expected to have significant sp^3 character. Hence the barrier to the loss of resonance stabilisation is sufficient to prevent R1 collapsing to a true tetrahedral oxyanion.

The optimisation of point MIN was restarted from the conformation of the doubly hydrogen-bonded structure MIN taken from the ester model. (The amide was initially modelled as planar in this structure.) This optimised to the structure described as MIN in Tables 1 and 2, in which the two hydrogen bonds to His-48 are somewhat distorted (the hydrogen bond lengths of H^T to O^H and N are 1.59 and 2.38 Å respectively, with an H^T–N^D–C^G angle of 122°). In contrast, the ester forms an oxyanion in which the hydrogen bonds are similar (1.86 and 2.02 Å for H^T–O^H and H^T–O^M respectively, with an angle of 125° for H^T–N^D–C^G). For the amide, points MIN and R1 are

very similar with respect to their position within the active site. However, MIN does represent a small movement of the oxyanion nitrogen towards His-48, *i.e.* on a suitable trajectory to receive H^T.

Point MIN was used as the starting structure for the optimisation of point P1 (*i.e.* with stretch of the C–N bond to 1.55 Å). P1 converged to a structure slightly higher in energy than MIN, but one where H^T was still more strongly bound to O^H than N. Starting a further optimisation with H^T initially positioned closer to N did not change the outcome of the optimisation. Points P2 and P3 also converged to similar structures, *i.e.* in which H^T remained closer to O^H than N; however, when these optimisations were started with a stretched H^T–N^D length, both converged to lower energy structures in which proton transfer to N was complete. Thus the proton transfer of H^T from His-48 to the oxyanion nitrogen is seen to occur much earlier for the amide oxyanion than for the ester oxyanion (*i.e.* at a C–N distance of between 1.55 and 1.65 Å, compared with a C–O^M distance of between 1.75 and 1.85 Å). This may result from the increased basicity of the amide nitrogen, as it re-hybridises from a non-basic sp^2 to a strongly basic sp^3 nitrogen.

Energetics of Amide Hydrolysis.—The energies of the amide oxyanion–imidazolium system *in situ* and *in vacuo* are described in Table 3 and in Figs. 5 and 6. For the *in situ* potential energy surface, ΔE_{TOT} is the sum of ΔE_{QM} and ΔE_{MM}: ΔE_{QM} is the QM energy of the QM system within the field of charges, and therefore includes the effect of polarisation of the wavefunction by the charges, and the nuclear repulsion between the QM nuclei and the point charges; ΔE_{MM} is the MM energy of interaction between QM and MM atoms, in terms of standard AMBER bonded and non-bonded energies (but excluding all electrostatic terms). ΔE_{QM} is calculated with the 3-21G basis set. For comparison, an estimate of the *in vacuo* potential energy surface was obtained by evaluating the QM energy of the oxyanion–imidazole couple in the absence of the point charge field: the structures were the same as for the *in situ* calculation (*i.e.*, no attempt was made to re-optimise the structures *in vacuo*). The *in vacuo* energies were calculated at the 4-31G basis set, to enable comparison with the energies calculated in ref. 9.

The earlier results for ester hydrolysis (shown for comparison in Figs. 5 and 6) highlight the large barrier to the formation of the oxyanion *in vacuo*, which is removed *in situ* by the favourable electrostatic interaction with calcium and the environment of the active site. The *in situ* curve shows a marked minimum for the formation of the oxyanion, rather than the essentially flat surface which would be expected. However, there are several reasons why the calculations should exaggerate the stability of the oxyanion. The most significant source of error will be the use of the 3-21G and 4-31G basis sets. Our earlier calculations have demonstrated that these basis sets will significantly underestimate the barrier to ester hydrolysis (by approximately 10–15 kcal mol^{-1})† when compared with a higher level of theory (the 6-31G** basis set with electron correlation estimated at the level of second order Moller-Plesset perturbation theory).[12] A further discrepancy will arise in the use of a field of static charges, which neglects the polarisation of the MM atoms by themselves and by the QM atoms, which may be an important factor in the shielding of the charges which develop on the oxyanion and imidazolium. It is also worth noting that the MM parameters themselves are of limited accuracy: the electrostatic interaction between the metal and the oxyanion is very large, and any small discrepancy in the ligand distance will significantly affect the total energy.

† 1 cal = 4.18 J.

However, a small minimum in ΔE_{QM} may well arise *in situ*, in order to negate any barrier in ΔE_{MM}. Although in this example ΔE_{MM} is small, it is possible that when a full-sized phospholipid forms the oxyanion intermediate, there is a greater steric interaction with the active site, including some torsional strain within the lipid itself.[12]

For the case of amide hydrolysis, it is seen that the attack of water on the substrate (points R5 to MIN) is accompanied by a small barrier in ΔE_{TOT}, in contrast with the marked minimum for ester hydrolysis: the potential energy surface shows a maximum at point R2, of 3.4 kcal mol^{-1} relative to R5. This barrier reflects the resonance stability of the amide linkage: as described above, point R1, in which the amide linkage remains nearly planar, was found to be a stable minimum, notwithstanding the stretched C–O^H bond. However, when the planarity of the amide is lost (point MIN has a dihedral of −88° for the amide linkage) there is a significant fall in the energy of the oxyanion.

The energy of the system increases between points P1 and P5, such that point P5 is 7.7 kcal mol^{-1} higher in energy than R5. This contrasts with the example of ester hydrolysis, where reactants and products were very similar in energy. However, for amide hydrolysis, there is a significant difference between the nature of the reactants (amide + water) and the products (methylamine + formic acid). Thus it may be expected that the reactant amide will bind more strongly to calcium than formic acid.[12] However, a more significant effect may be due to the basis set dependency of the results. In earlier calculations[12] we have noted that the 3-21G and 4-31G basis sets reproduce the barrier to amide hydrolysis fairly accurately when compared with 6-31G**/MP2 calculations, whereas they significantly underestimate the barrier to ester hydrolysis. Therefore it is to be expected that the energy of the oxyanion (MIN) relative to the reactants will be accurately evaluated whereas the stability of MIN relative to the products will be exaggerated.

The various oxyanion–imidazolium structures of points R5–P5 were evaluated at 4-31G *in vacuo*, *i.e.* with no environment present. Fig. 6 shows the large barrier to the formation of the oxyanion *in vacuo* (+33 kcal mol^{-1}), which is greater than that of ester hydrolysis. Note that R1 is the point highest in energy; there is a large fall in energy to MIN and then a very small barrier at P1 before the fall to the products, P5. (Again the products are higher in energy than the reactants, by 9.3 kcal mol^{-1}, which is probably the effect of the basis set.)

These results highlight the expected difference between amide and ester hydrolysis. As suggested by Komiyama and Bender for the case of the serine proteases,[19] the rate-limiting step to amide hydrolysis is the attack of water on the amide to form the oxyanion; at this point, the planarity of the amide is lost, and so proton transfer from histidine to the strongly basic sp^3 nitrogen should proceed rapidly. This is seen in the *in vacuo* results above, but is perhaps lost in the *in situ* results, where a probably flat potential energy surface between MIN and P5 becomes an uphill path because of the limitations in the basis set. The rapid decomposition of the amide oxyanion in other hydrolytic enymes may provide a reason for the scant experimental evidence for such an intermediate, while there is evidence of the existence of the ester oxyanion intermediate.[17,19] Similar energetics have been calculated for a model of ester/amide hydrolysis in trypsin.[25]

Estimated in situ *Transition State for Proton Transfer.*—As the reaction path from R5 to MIN showed a distinct maximum *in situ*, a saddle point calculation was performed to locate the transition state *in situ* for the proton transfer of H^T from O^H to N^D and for the formation of the C–OH bond. As a starting structure for the calculation, the point R2 was chosen, with H^T adjusted to lie midway between N^D and O^H. A saddle optimis-

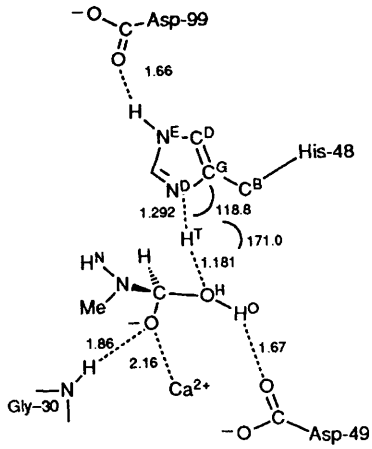

Fig. 7 The structure of the estimated transition state for amide hydrolysis (model TS) within the active site. Interatomic distances are quoted in ångströms, angles in degrees.

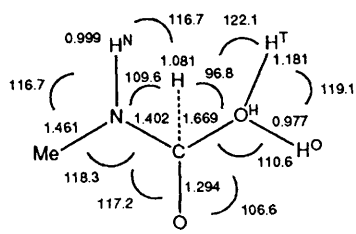

Angles

H–C–O	118.5	N–C–O^H	105.0

Dihedrals

Me–N–C–O^H	−77.6	Me–N–C–O	40.5	Me–N–C–H	179.4
N–C–O^H–H^O	121.4	H^N–N–C–O	−172.2	H^T–O^H–C–O	−151.8
O^H–H^T–N^D–C^G	−19.6				

Fig. 8 3-21G optimised geometry of the estimated transition state for amide hydrolysis (model TS) within the active site. Lengths are quoted in ångströms, angles in degrees.

ation was attempted, following the Jorgensen and Simons algorithm,[26] which made use of combined QM–MM gradients as in the earlier optimisations. The saddle optimisation converged readily (to the same tolerance as for the earlier optimisations, *i.e.* the maximum gradient below 0.001 hartree $bohr^{-1}$). The final Hessian (the matrix of second derivatives of the energy with respect to the coordinates) was of the required structure for a transition state, *i.e.* with one negative eigenvalue. However, this cannot be taken as confirmation that a true transition state has been reached, as this Hessian is updated during the optimisation procedure and the true Hessian is never recalculated. Confirmation of the eigenvalues by re-calculation of an analytical or numerical Hessian was not feasible because of the larger number of variables, as well as practical limitations within the program, and so the observed saddle point was not proven to be a true transition state.

The structure of this point (labelled TS) is described in Figs. 7 and 8, and in Tables 1 and 2. The C–OH bond length of 1.67 Å is slightly longer than in point R2, and it may be seen that all geometries of point TS are intermediate between those of structures R2 and R3. In TS, H^T is midway between N^D and O^H, although closer to the latter (1.29 *versus* 1.18 Å). The N^D–H^T–O^H angle is approximately linear (171°).

The energy (E_{TOT}) of point TS is +4.3 kcal mol^{-1} higher than R5, or +0.9 kcal mol^{-1} higher than the maximum in the potential curve, R2. Although point TS would be expected to be similar in energy to R2, it is likely that, with such a complex potential energy surface, point TS is not on exactly the same trajectory as R3 and R2; any small difference in position may be reflected by a significant change in the large electrostatic interaction of the oxyanion with imidazolium and the calcium charge. The energy of TS *in vacuo* is +24.4 kcal mol^{-1} higher than R5; thus TS lies on the curve (Fig. 6) between R3 and R2 and does not represent a maximum *in vacuo*.

This saddle point optimisation has demonstrated that the hybrid QM–MM method is a practical means of finding a transition state within a complex macromolecular environment. However, in this example it has not been possible to confirm that the optimised structure is a true transition state. In any case, the nature of such a transition state will be very sensitive to the presence of constraints on the system (in this case, the limited movement of the imidazolium ring), to the nature of the MM environment and to the choice of basis set. Therefore the final structure is no more than an estimation of the transition state within the limitations of the model and the level of theory which has been used. Even so, the structure appears to be a reasonable one, with all geometric variables between those of R2 and R3. With respect to the mechanism of amide hydrolysis, the structure again confirms that attack of water on the substrate is concerted with proton transfer to imidazole.

Implications for the Mechanism of Amide Hydrolysis.—The present calculations demonstrate that the reaction path for amide hydrolysis within the active site of PLA2 is in general similar to that for ester hydrolysis. It is known experimentally that an amide phospholipid will bind strongly to PLA2 but is not hydrolysed.[18] The results suggest that this is due to the relative barriers to hydrolysis of the two substrates. The *in vacuo* potential energy surfaces demonstrate the large barrier to amide hydrolysis which is a result of the resonance stability of the amide linkage. *In situ*, the environment of the active site serves to reduce this barrier for both ester and amide substrates, although ester hydrolysis remains more favourable. Although the difference in ester and amide reactivity is here exaggerated by the choice of basis set, our earlier calculations have shown that a similar outcome is seen even with the use of large polarised basis sets and with the inclusion of electron correlation.

It is worth noting that these calculations are intended as a method to investigate structural and energetic aspects of the potential energy surface of proton transfer, and not specifically as a means of defining the barrier to substrate hydrolysis. In particular, it is the case that only a small region of the reaction path has been examined, *i.e.* for a separation of reactants or products of 2 Å. If the potential energy surface were extended, there may well be a larger difference in the barriers to amide and ester hydrolysis *in situ*.

In summary, the mechanisms of amide and ester hydrolysis both involve a similar transfer of a proton from the nucleophilic water to the products, *via* His-48. The rate-limiting step may well be different in each case, however. Thus in the case of amide hydrolysis, proton transfer from water to His-48 is delayed (relative to ester hydrolysis) while proton transfer from His-48 to products occurs much earlier.

Conclusions

A hybrid QM–MM methodology has been used to investigate the potential energy surfaces of ester and amide hydrolysis within a model of the active site of PLA2. The calculations highlight the usefulness of the method in the generation of transition structures along a reaction path, where the geometry and energy of the structures are dependent on the electrostatic and steric interactions with a macromolecular environment.

The results are in agreement with the proposed mechanism of hydrolysis by PLA2. Proton transfer from the nucleophilic water to His-48 and thence to the oxyanion is seen to be a

feasible mechanism, in that the reaction path is energetically favourable and requires no significant distortion of the substrate or His-48. The results have demonstrated differences in energetics and mechanism between ester and amide hydrolysis.

Clearly, there are many approximations in the methodology which limit the accuracy of the results. The use of a small active-site model, which is not allowed to move in response to structural changes in the substrate, is likely to be a minor source of error. More serious limitations arise from the choice of basis set, which significantly affects the relative stabilities of amide and ester, and from the treatment of the electrostatic potential of the MM atoms, which are not allowed to be polarised by themselves or by changes in the charge distribution of the QM atoms. The correction of both of these failings requires a considerable increase in computational expense, but clearly must be addressed in the future if such a hybrid QM–MM method is to produce results of a quantitative accuracy. Therefore it should be stressed that the calculated structures and energies are dependent on the model which has been used. Alterations to the MM environment or the use of a different basis set may well influence some of the findings: for example, the point at which proton transfer occurs will be dependent on the stability of the ionic oxyanion–imidazolium couple within the particular model which is chosen.

However, even with these limitations, this remains a valuable method to optimise a structure at a QM level within a macromolecular environment. As has been discussed, no method which uses QM alone is capable of describing the electrostatic and steric nature of the bulk environment, or of allowing the optimisation of the oxyanion–imidazolium system while retaining so many degrees of freedom. Thus, the optimisation of these structures would not have been possible by a standard MO or MM method alone. The hybrid QM–MM method is not necessarily applicable to all examples where a small substrate is to be optimised in a complex environment. For example, it is less appropriate for a reaction path within bulk solvent, where it may be vital to simulate simultaneous movement of the solvent molecules in response to changes in the geometry of the solute. The cases presented here are a better example of the use of the method in its current form, where the environment of an enzyme active site can be assumed to be immobile with respect to small structural changes of the substrate. Further development of these hybrid methods may be able to overcome some of the present limitations.

Acknowledgements

We thank the SERC for support of this research under grants GR/E53682 and GR/F49934.

References

1 (*a*) G. Bolis, M. Ragazzi, D. Salvaderi, D. R. Ferro and E. Clementi, *Gazz. Chim. Ital.* 1978, **108**, 425; (*b*) G. Alagona, P. Desmeules, C. Ghio and P. A. Kollman, *J. Am. Chem. Soc.*, 1984, **106**, 3623; (*c*) S. J. Weiner, G. L. Seibel and P. A. Kollman, *Proc. Natl. Acad. Sci. USA*, 1986, **83**, 649; (*d*) D. Arad, R. Langridge and P. A. Kollman, *J. Am. Chem. Soc.*, 1990, **112**, 491.

2 (*a*) R. Broer, P. T. van Duijnen and W. C. Niewpoort, *Chem. Phys. Lett.*, 1976, **42**, 525; (*b*) D. Demoulin and A. Pullman, *Theor. Chim. Acta*, 1978, **49**, 161; (*c*) S. Nakagawa, H. Umeyama and T. Kudo, *Chem. Pharm Bull.*, 1980, **28**, 1342; (*d*) P. A. Kollman and D. M. Hayes, *J. Am. Chem. Soc.*, 1981, **103**, 2955; (*e*) R. Osman, H. Weinstein and S. Topiol, *Ann. NY Acad Sci.*, 1981, **367**, 356.

3 A. Warshel and M. Levitt, *J. Mol. Biol.*, 1976, **103**, 227.

4 (*a*) A. Warshel and R. M. Weiss, *J. Am. Chem. Soc.*, 1980, **102**, 6218; (*b*) A. Warshel and F. Sussman, *Proc. Natl. Acad. Sci. USA*, 1986, **83**, 3806; (*c*) J. Åqvist and A. Warshel, *Biochemistry*, 1989, **28**, 4680.

5 U. C. Singh and P. A. Kollman, *J. Comput. Chem.*, 1986, **7**, 718.

6 (*a*) P. A. Bash, M. J. Field and M. Karplus, *J. Am. Chem. Soc.*, 1987, **109**, 8092; (*b*) M. J. Field, P. A. Bash and M. Karplus, *J. Comput. Chem.*, 1990, **11**, 700.

7 P. K. Weiner and P. A. Kollman, *J. Comput. Chem.*, 1981, **2**, 287.

8 (*a*) D. M. Hayes and P. A. Kollman, *J. Am. Chem. Soc.*, 1976, **98**, 7811; (*b*) L. C. Allen, *Ann. NY Acad. Sci.*, 1981, **367**, 383; (*c*) S. Nakagawa and H. Umeyama, *J. Theor. Biol.*, 1982, **96**, 473; (*d*) H. Umeyama, S. Hirono and S. Nakagawa, *Proc. Natl. Acad. Sci. USA*, 1984, **81**, 6266.

9 B. Waszkowycz, I. H. Hillier, N. Gensmantel and D. W. Payling, *J. Chem. Soc., Perkin Trans. 2*, 1991, 225.

10 A. J. Slotboom, H. M. Verheij and G. H. de Haas, *New Compr. Biochem.*, 1982, **4**, 354.

11 J. Chang, J. H. Musser and H. McGregor, *Biochem. Pharmacol.*, 1987, **36**, 2429.

12 (*a*) B. Waszkowycz, I. H. Hillier, N. Gensmantel and D. W. Payling, *J. Chem. Soc., Perkin Trans. 2*, 1989, 1795; (*b*) B. Waszkowycz, I. H. Hillier, N. Gensmantel and D. W. Payling, *J. Chem. Soc., Perkin Trans. 2*, 1990, 1259.

13 H. M. Verheij, J. J. Volwerk, E. H. Jansen, W. C. Puyk, B. W. Dijkstra, J. Drenth and G. H. de Haas, *Biochemistry*, 1980, **19**, 743.

14 B. W. Dijkstra, K. H. Kalk, W. G. J. Hol and J. Drenth, *J. Mol. Biol.*, 1981, **147**, 97.

15 M. M. G. M. Thunnissen, E. Ab, K. H. Kalk, J. Drenth, B. W. Dijkstra, O. P. Kuipers, R. Dijkman, G. H. de Haas and H. M. Verheij, *Nature (London)*, 1990, **347**, 689.

16 D. L. Scott, S. P. White, Z. Otwinowski, W. Yuan, M. H. Gelb and P. B. Sigler, *Science*, 1990, **250**, 1541.

17 (*a*) A. A. Kossiakof and S. A. Spencer, *Biochemistry*, 1981, **20**, 6462; (*b*) T. A. Steitz and R. G. Shulman, *Ann. Rev., Biophys. Bioeng.*, 1982, **11**, 419.

18 G. H. de Haas, M. G. van Oort, R. Dijkman and R. Verger, *Biochem. Soc. Trans.*, 1989, **17**, 274.

19 M. Komiyama and M. L. Bender, *Proc. Natl. Acad. Sci. USA*, 1979, **76**, 557.

20 M. F. Guest and J. Kendrick, GAMESS User Manual, CCP1/86/1, Daresbury Laboratory, UK, 1986.

21 P. B. Hitchcock, R. Mason, K. M. Thomas and G. G. Shipley, *Proc. Natl. Acad. Sci. USA*, 1974, **71**, 3036.

22 S. J. Weiner, P. A. Kollman, D. T. Nguyen and D. A. Case, *J. Comput. Chem.*, 1986, **7**, 230.

23 S. J. Weiner, P. A. Kollman, D. A. Case, U. C. Singh, C. Ghio, G. Alagona, S. Profeta and P. Weiner, *J. Am. Chem. Soc.*, 1984, **106**, 765.

24 U. C. Singh and P. A. Kollman, *J. Comput. Chem.*, 1984, **5**, 129.

25 S. Nakagawa and H. Umeyama, *J. Mol. Biol.*, 1984, **179**, 103.

26 (*a*) J. Simons, P. Jorgensen, H. Taylor and J. Ozment, *J. Phys. Chem.*, 1983, **87**, 2745; (*b*) A. Banerjee, N. Adams, J. Simons and R. Shepherd, *J. Phys. Chem.*, 1985, **89**, 52; (*c*) J. Baker, *J. Comput. Chem.*, 1986, **7**, 385.

Paper 1/03647E
Received 18*th July* 1991
Accepted 5*th September* 1991